


Article

Enhanced Two-Photon Fluorescence and Fluorescence Imaging of Novel Probe for Calcium Ion by Self-Assembly with Conjugated Polymer

Yue-liang Zhai ^{1,2,†}, Qiu-bo Wang ^{1,2,†}, Hao Yu ^{1,2}, Xiao-yuan Ji ^{1,2} and Xian Zhang ^{1,2,*} 

¹ School of Materials Science and Engineering, Qilu University of Technology (Shandong Academy of Sciences), Jinan 250353, China; zhaiyuelianger@163.com (Y.-l.Z.); wangqbqlu18@163.com (Q.-b.W.); yh15215425480@163.com (H.Y.); jixy0430@163.com (X.-y.J.)

² Shandong Provincial Key Laboratory of Processing and Testing Technology of Glass and Functional Ceramics; Key Laboratory of Amorphous and Polycrystalline Materials; Qilu University of Technology, Jinan 250353, China

* Correspondence: zhangx@qlu.edu.cn; Tel.: +86-531-8963-1227

† The authors (Y.-l.Z. and Q.-b.W.) contributed equally to this work.

Received: 31 August 2019; Accepted: 5 October 2019; Published: 10 October 2019



Abstract: The calcium ion (Ca^{2+}) is a highly versatile intracellular signal messenger regulating many different cellular functions. It is important to design probes with good fluorescence and two-photon (TP) active cross-sections ($\Phi\delta$) to explore the concentration distribution of Ca^{2+} . In this manuscript, a novel TP fluorescence calcium probe (BAPTAVP) with positive charges, based on the classical Ca^{2+} indicator of BAPTA (1,2-bis(2-aminophenoxy)-ethane-*N,N,N',N'*-tetraacetic acid), and a conjugated polymer (PCBMB) with negative charges were designed and synthesized. The results from transmission electron microscopy (TEM), atomic force microscopy (AFM), dynamic light scattering (DLS), and the zeta potential (ZP) showed that nanoparticles were obtained by the self-assembly of PCBMB and BAPTAVP. Moreover, the fluorescence properties of BAPTAVP were effectively improved by fluorescence resonance energy transfer (FRET) with PCBMB and attenuating the intramolecular charge transfer (ICT) after the addition of Ca^{2+} . The quantum yield and $\Phi\delta$ of PCBMB-BAPTAVP increased by about four and six times in comparison to those of BAPTAVP, respectively. The TP fluorescence imaging experiments indicated that the PCBMB-BAPTAVP system could effectively detect Ca^{2+} in living cells with high sensitivity.

Keywords: fluorescence probe; Ca^{2+} ; conjugated polymer; self-assembly; two-photon fluorescence imaging

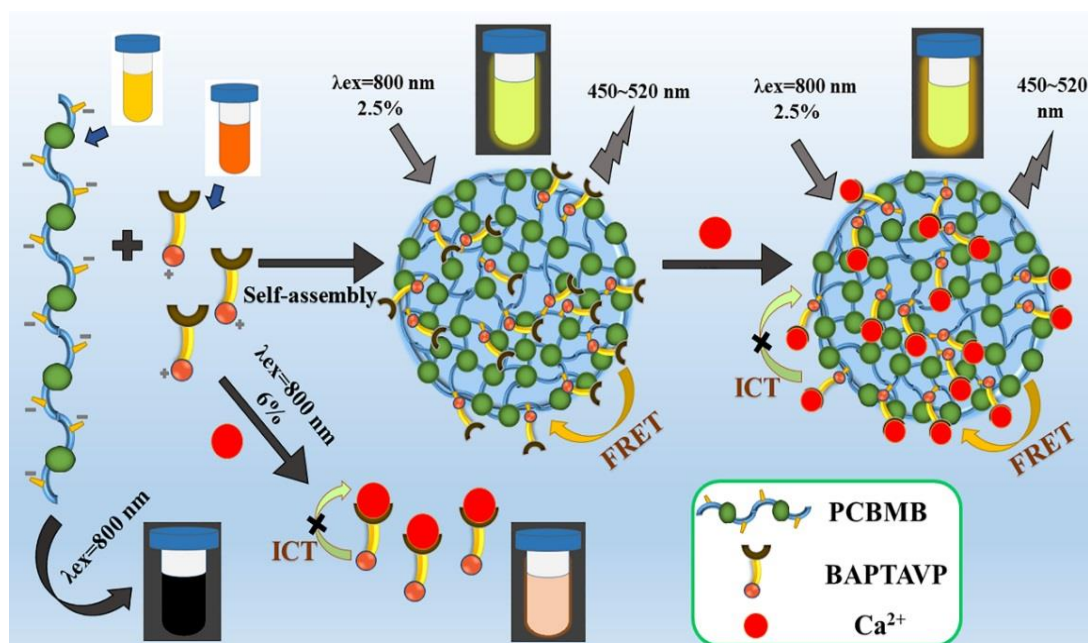
1. Introduction

Recently, research about selective and sensitive fluorescent indicators for metal ions has attracted significant attention [1–3], because metal ions play indispensable roles in a variety of fundamental physiological processes in organisms. The calcium ion, Ca^{2+} , is a highly versatile intracellular signal messenger regulating many different cellular functions [4,5], such as sensory transduction, exocytosis, muscle contraction, and enzyme activity [6,7]. The change in Ca^{2+} concentrations and the translocation of Ca^{2+} across the plasma membrane have often been used to explore these functions [8]. At present, two-photon microscopy (TPM) combined with suitable probes exhibits better localized excitation, much less photon damage and photobleaching [9], a small absorption coefficient of light in tissue, and lower tissue autofluorescence [10], and is often used to study Ca^{2+} in living cells. Although a few two-photon (TP) fluorescence probes such as ACalN have been developed [11], and their properties are far superior to previous one-photon (OP) fluorescence ones, such as Mag-Fura-2 and Calcium

Green C₁₈ applied in TPM, the TP active cross-sections ($\Phi\delta$) of these probes are still not very ideal [12]. Thus, it is important to develop new suitable probes with larger $\Phi\delta$ using the simple method.

As we all know, conjugated polymers (CPs), as an important type of TP material, exhibit good fluorescent properties. They usually have the advantages of a large Stokes shift, high quantum yield (Φ), excellent optical stability, and reasonable application prospects in the field of fluorescence imaging [13,14]. However, their targeting has been questioned, limiting further application [15–17], whereas many small organic molecules have exhibited a high performance at recognizing the targets [18,19]. Thus, we think it is possible to improve the TP properties of dyes by combining small molecules with CPs. At present, some novel two-photon fluorescence sensing platforms based on fluorescence resonance energy transfer (FRET) between the dyes and CPs have been designed to achieve better fluorescence properties [20,21]. Zhang et al. obtained a novel fluorescent probe by FRET between gold and conjugated polymer nanoparticles. The probe was highly sensitive and selective to melamine and has been successfully applied to milk powder [22]. Sha et al. designed a spirolactam rhodamine-linked adamantane as a ratiometric sensor for Hg²⁺. The fluorescence was effectively enhanced by FRET on the polymer brush-functionalized mesoporous silica nanoparticles with CPs [23]. However, few studies have detected Ca²⁺ based on the polymers by two-photon excitation. It may be a strategy to improve the TP properties of dyes by combining small molecules with CPs.

Herein, a new TP probe (BAPTAVP) with positive charges based on the traditional indicator of Ca²⁺ with high selectivity and sensitivity was synthesized and characterized. Nanoparticles were formed by self-assembly with the conjugated polymer of a carbazole derivative (PCBMB) with negative charges and BAPTAVP with positive charges. Moreover, TP fluorescent properties of BAPTAVP were effectively improved by FRET with PCBMB and attenuating the intramolecular charge transfer (ICT) after the addition of Ca²⁺. The key diagram is displayed in Scheme 1. Furthermore, TPM for the detection of Ca²⁺ in living cells was finished successfully. It may provide a new method to improve the TP properties of some traditional fluorescence probes and further widen their applications.



Scheme 1. Mechanism diagram of enhanced fluorescence based on self-assembly between PCBMB and BAPTAVP.

2. Experimental

2.1. Chemicals and Instruments

All chemicals were obtained from commercial suppliers and used without further purification. Ultrapure water was used in all experiments. A solution of Ca^{2+} was prepared from their nitrate salts.

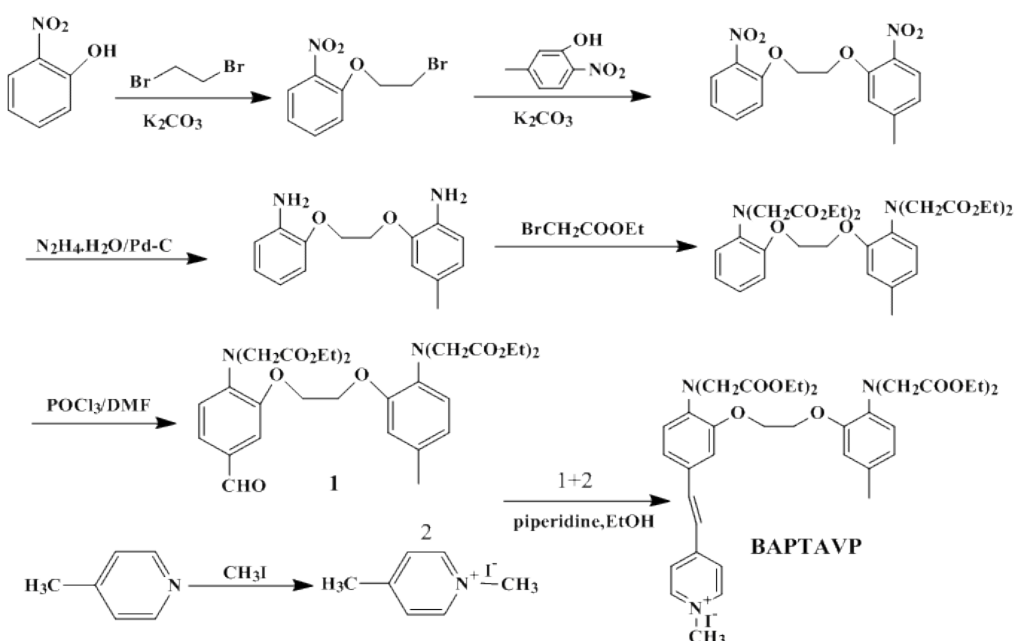
^1H NMR spectra were recorded on a Bruker AvanceII 400 spectrometer using TMS as an internal standard. The element analyses were performed on a Perkin 2400 (II) autoanalyzer. Infrared spectra were recorded on a Nicolet NEXUS 670 FT-IR spectrometer using a liquid-nitrogen-cooled detector. UV-vis absorption spectra were recorded on a Varian Cary 50 spectrophotometer using a quartz cuvette with a 1 cm path length. The pH values were measured with a Mettler-Toledo FE20 pH meter. One-photon fluorescent spectra were recorded with a HITRCHIF-7000 fluorescence spectrometer. Two-photon fluorescent spectra were recorded on an OOIBASE32 spectrophotometer. The pump laser beam was from a mode-locked Ti:Sapphire laser system with a pulse duration of 200 fs, a repetition rate of 76 MHz, and a wavelength range of 700–1000 nm (Coherent Mira900-D). Transmission electron microscopy (TEM) images were recorded through a JEM-2100 electron microscope (JEOL Ltd., Musashino, Japan). Atomic force microscopy (AFM) was performed on a Multimode8. Dynamic light scattering (DLS) and zeta potential (ZP) data were obtained on a Malvern Zetasizer Nano ZS analyzer (Malvern, Worcestershire, UK). Fluorescence images of SiHa cells were obtained using a Zeiss Ism710 laser confocal microscope.

2.2. Synthesis

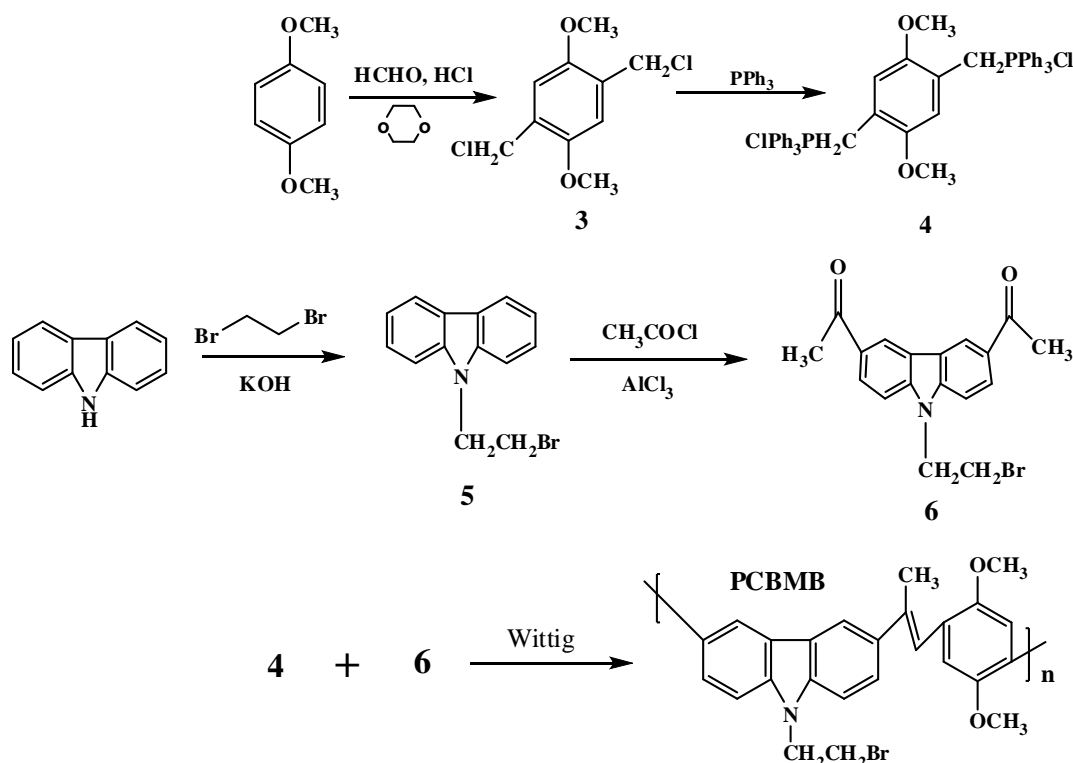
For the synthesis details of 5-formyl-5'-methyl-BAPTA ethyl ester (**1**) (BAPTA: 1,2-bis(2-aminophenoxy)-ethane- N,N,N',N' -tetra acetic acid) and 4-methyl- N -methyl pyridine iodized salt (**2**), see the relevant literature [24,25].

We obtained 1,4-bis(chloromethyl)-2,5-dimethoxybenzene (**3**), and [(2,5-dimethoxy-1,4-phenylene) bis-(methylene)]bistriphenylphosphonium dichloride (**4**) as described in the literature [26]. The synthesis process of N -bromoethyl-carbazole (**5**) was referred in the literature [27].

The synthetic routes of BAPTAVP and PCBMB are shown in Schemes 2 and 3, respectively.



Scheme 2. Synthetic route of BAPTAVP.



Scheme 3. Synthetic route of PCBMB.

2.2.1. Procedure for the Synthesis of 5-(4-vinyl-N-methyl pyridine iodized salt)-5'-Methyl-BAPTA Ethyl Ester (BAPTAVP)

Aldehyde derivative 1 (1 g, 1.587 mmol) and iodized salt 2 (0.39 g, 1.66 mmol) were dissolved in ethyl alcohol (30 mL). After adding 10 drops of piperidine, the mixture was slowly heated to 80 °C and stirred for 10 h, followed by cooling to room temperature. After filtering and washing with water and methanol, the crude product was obtained and then recrystallized to give yellow crystals with a yield of 47.3%. ¹H NMR (CDCl₃, 400 MHz, TMS) δ (ppm): 8.54 (d, *J* = 7.2 Hz, 2 H), 8.03 (d, *J* = 6.8 Hz, 2 H), 7.25 (m, 4 H), 6.76 (m, 4 H), 4.21 (m, 20 H), 2.28 (s, 3 H), 1.94 (s, 3 H), 1.18 (t, *J* = 22 Hz, 12 H). IR (KBr) ν /cm⁻¹: 1632 cm⁻¹ (C=C); 1253 cm⁻¹ (C-N); 1591 cm⁻¹ (C=N); 2928 cm⁻¹, 2994 cm⁻¹ (-CH₃); 1738 cm⁻¹ (C=O); 1009 cm⁻¹ (C-O). Element analysis calcd (%) for C₃₉H₅₀N₃O₁₀I: C 55.25, H 5.90, N 4.96; found: C 55.38, H 5.88, N 4.98.

2.2.2. Procedure for the Synthesis of 3,6-bis-(methyl ketone)-N-bromoethyl-carbazole (6)

In a three-necked bottle, anhydrous aluminum trichloride (0.813 g, 7.10 mmol) was dissolved in 1,2-dichloroethane (13.5 mL) and then cooled to 5 °C. Acetyl chloride (0.96 g, 12.2 mmol) was added to the mixture in two minutes. Compound 5 (1.4 g, 5.30 mmol) dissolved in 1,2-dichloroethane was dropwise added into the reactive solution and stirred for 20 min. Then, the mixture was warmed up to 35 °C and stirred for another 2.5 h. The solvent was removed under reduced pressure. The mixture was neutralized with diluted hydrochloric acid (15 mL) and filtered to afford pale yellow powders, and then recrystallized from ethanol. ¹H NMR (CDCl₃, 400 MHz, TMS) δ (ppm): 8.80 (s, 2 H), 8.20 (d, *J* = 10.4 Hz, 2 H), 7.51 (d, *J* = 8.4 Hz, 2 H), 4.79 (t, *J* = 14.4 Hz, 2 H), 3.75 (t, *J* = 14 Hz, 2 H), 2.76 (s, 6 H).

2.2.3. Procedure for the Synthesis of the Conjugated Polymer (PCBMB)

A mixture including compound 4 (0.758 g, 0.997 mmol), compound 6 (0.36 g, 1.05 mmol), and chloroform (10 mL) was added to a three-necked bottle and stirred for 30 min at room

temperature (r.t.) under nitrogen atmosphere. Potassium tert-butoxide (1 g, 8.93 mmol) dissolved in ethanol was dropwise added to the mixture and stirred for 2 days at r.t., and the solvent was then removed under reduced pressure. The residue was dissolved in dichloromethane and stirred for 10 min, then filtered. The yellow powders were obtained after washing with methyl alcohol three times with a yield of 30.4%. $^1\text{H NMR}$ (CDCl_3 , 400 MHz, TMS) δ (ppm): 8.78 (s, 2 H), 8.18 (d, $J = 10.4$ Hz, 2 H), 7.69 (d, $J = 8.4$ Hz, 2 H), 7.28 (s, 2 H), 6.69 (m, 1 H), 5.70 (d, $J = 16.8$ Hz, 1 H), 5.45 (d, $J = 10$ Hz, 1 H), 3.70 (m, 2 H), 2.76 (s, 6 H). IR (KBr) ν/cm^{-1} : 3005 cm^{-1} (C–H); 1267 cm^{-1} (C–N); 2949 cm^{-1} , 3001 cm^{-1} (CH_3); 1686 cm^{-1} (C=O); 1675 cm^{-1} (C=C); 1044 cm^{-1} (C–O); 626 cm^{-1} (C–Br). $M_w/M_n = 1.326$, $M_z/M_n = 1.809$; $M_n = 5127$; $M_w = 5820$; $M_z = 6848$ (GPC, polystyrene calibration).

2.3. Preparation of Solutions and Spectral Measure

The stock solutions of Ca^{2+} in the ultrapure water and BAPTAVP were prepared in tris-HCl buffer solution (10 mmol/L, KCl 100 mmol/L, pH 7.2) with a concentration of 2×10^{-2} mol/L. The stock solution of PCBMB (1×10^{-3} mol/L) was prepared in THF. Test sample solutions were diluted to the appropriate concentrations using tris-HCl buffer solution, and the spectra were then measured after adding acetylcholin esterase and placed for 20 min. The OP and TP fluorescence spectra were excited at 264 nm (for PCBMB), 420 nm (for BAPTAVP), and 800 nm, respectively. The $^1\text{H NMR}$ of three samples including pure BAPTAVP, BAPTAVP-added acetylcholin esterase, BAPTAVP-added acetylcholin esterase, and Ca^{2+} was measured in CDCl_3 .

2.4. General Processes for Cell Culture and Fluorescence Imaging

SiHa cells were grown in H-DMEM (Dulbecco's Modified Eagle's Medium, High Glucose) supplemented with 10% FBS (fetal bovine serum) in a 5% CO_2 incubator at 37 °C. Cells (1×10^5 / mL) were placed on glass coverslips and allowed to adhere for 24 h. The living SiHa cells were incubated with 5 $\mu\text{mol/L}$ solution of BAPTAVP, BAPTAVP- Ca^{2+} , PCBMB-BAPTAVP, and PCBMB-BAPTAVP- Ca^{2+} for 1 h at 37 °C, respectively, and were then washed with PBS three times to image. Two-photon fluorescence imaging was observed under a Zeiss Ism710 confocal microscope at 800 nm.

3. Results and Discussion

3.1. Design of BAPTAVP and PCBMB

The probe was designed on the basis of BAPTA (o,o'-bis(2-aminophenyl) ethyleneglycol-N,N,N',N'-tetra acetic acid), which is a well-known Ca^{2+} indicator that has been widely applied as OP fluorescence probes [28]. By introducing four ester groups (-Et), the penetrability of the probe into cells can be considerably improved [29,30]. The pyridine ring as an excellent electron acceptor was introduced into the structure. Biphenyl ethylene was chosen as the conjugated bridge owing to its good planarity. Meanwhile, in order to improve biocompatibility, the compound was converted to pyridine salt. The design of PCBMB was based on carbazole derivatives owing to its π -conjugated backbone. The delocalized system was further enlarged by introducing the benzene ring and conjugated double-bond by the Wittig reaction. The fluorescent intensity was further strengthened by connecting a strong electron donor of $-\text{OCH}_3$.

3.2. Linear and Nonlinear Spectra of BAPTAVP with Ca^{2+} Titration

Different volumes of Ca^{2+} were added to the solution of BAPTAVP in tris-HCl buffer solution (10 mmol/L, KCl 100 mmol/L, pH 7.2) with a concentration of 1×10^{-5} mol/L, and the mole concentration ratios of Ca^{2+} to BAPTAVP ($\text{Ca}^{2+}:\text{B}$) were 0, 0.2, 0.5, 1.0, 2.0, 3.0, 6.0, 10.0, 15.0, and 20.0. The absorption and OP fluorescence spectra are shown in Figure 1a,b, respectively. It can be observed that the changing trend of absorbance is almost coincident with that of the fluorescent intensity (upper right corner in Figure 1a,b). The absorbance and fluorescence obviously increase with the addition of Ca^{2+} before the ratio of $\text{Ca}^{2+}/\text{probe} = 1$, and then begin to decline and level off at the ratio of 8.0, which indicates that

a steady complex of Ca^{2+} /probe may have formed at the ratio of 1.0. Meanwhile, other coordinations of Ca^{2+} to BAPTAVP, such as a 2:1 or 3:1 complex (Ca/B), may appear to induce a change in fluorescence. A similar change trend was found in other research [31]. The fluorescent intensity of BAPTAVP exhibits a good linear relationship ($y = 1.43x + 46.7$, $R^2 = 0.991$) with the concentrations of Ca^{2+} in the range from 1×10^{-7} to 1×10^{-5} mol/L in Figure 1c. The limit of detection (LOD) of BAPTAVP for OP fluorescence was estimated to be 9.6×10^{-8} mol/L, which was obtained by the equation $\text{LOD} = 3S_b/K$ [32] (S_b represents the standard deviation and K is the slope between fluorescence intensity versus Ca^{2+} concentration). This value is superior to that reported in the literature in the detection of endogenous Ca^{2+} [33].

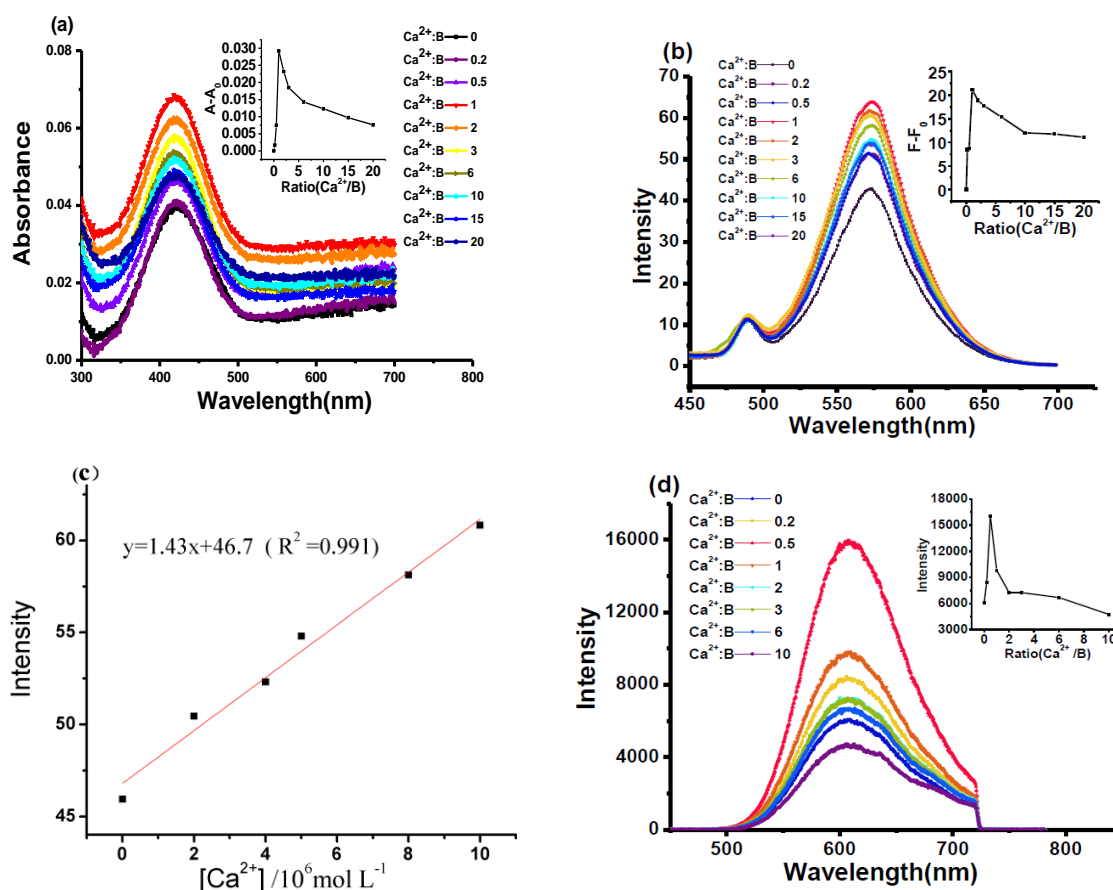


Figure 1. (a) Absorption spectra and (b) one-photon fluorescence emission spectra of BAPTAVP (B) in tris-HCl buffer solution upon 0–20 equiv. of $\text{Ca}(\text{NO}_3)_2 \cdot 4\text{H}_2\text{O}$ pre-dissolved in ultrapure water. Inset in upper right corner of (a) is the absorption at 420 nm evolution with Ca^{2+} concentrations; inset in upper right corner of (b) is the fluorescent intensity at 570 nm evolution with Ca^{2+} concentrations. (c) Linear fitting curve of the fluorescent intensity against the concentrations of Ca^{2+} ; (d) two-photon (TP) fluorescent emission spectra of the BAPTAVP in tris-HCl buffer solution upon 0–10 equiv. of $\text{Ca}(\text{NO}_3)_2 \cdot 4\text{H}_2\text{O}$ pre-dissolved in ultrapure water. In set in upper right corner of (d) is the plot of fluorescent intensity evolution with Ca^{2+} concentrations.

TP fluorescent spectra were investigated upon adding different volumes of Ca^{2+} to tris-HCl buffer solution with a concentration of 8×10^{-4} mol/L at 800 nm. The mole ratios of Ca^{2+} /probe were 0, 0.2, 0.5, 1.0, 2.0, 3.0, 6.0, and 10.0. The experimental results are displayed in Figure 1d. Compared to the original compound, no obvious red-shifts or blue-shifts were found with the increase in Ca^{2+} concentration. The changing trend of TP fluorescent intensity is similar to that of OP fluorescence. However, the fluorescent maximum point appeared at the ratio of Ca^{2+} /probe = 0.5, which is different from that of OP excitation. This may be attributed to the higher concentration (8×10^{-4} mol/L) of the dye under TP excitation, and this phenomenon was found in our previous reports [18,34].

3.3. Dissociation Constant of BAPTAVP/ Ca^{2+} Complex

The dissociation constant (K_d), which represents the connection between Ca^{2+} and the dye, was calculated. The K_d was calculated according to the following equation [28]:

$$\log [\text{Ca}^{2+}] = \log k_d + \log[(F - F_{\max}) / (F_{\min} - F)] \quad (1)$$

where F is the fluorescence intensity, F_{\max} is the maximum fluorescence intensity, F_{\min} is the fluorescence intensity in the absence of Ca^{2+} , and $[\text{Ca}^{2+}]$ is the free calcium ion concentration. The K_d value can be obtained from the fitting curve (see Figure 2a).

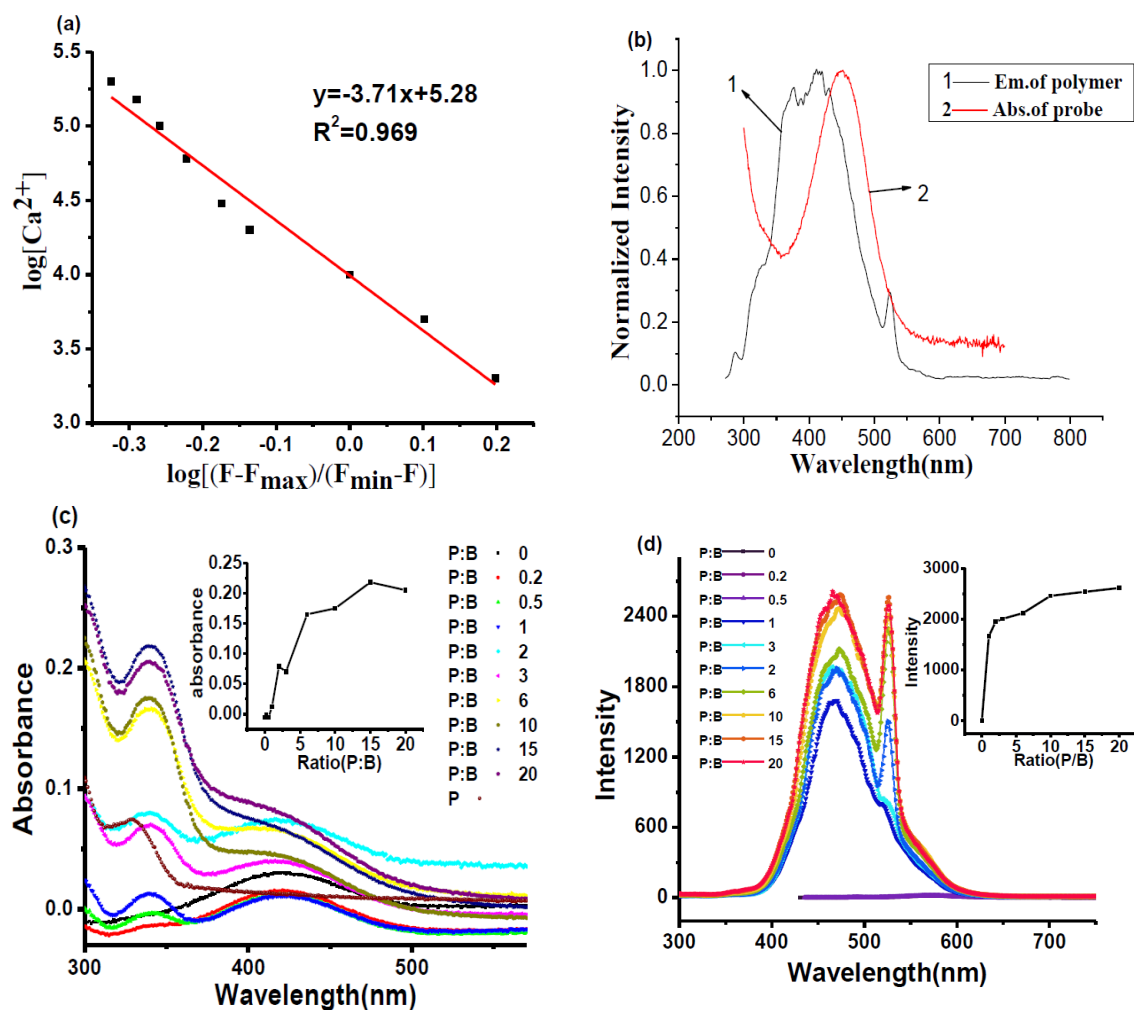


Figure 2. (a) Fitting curve of K_d between BAPTAVP and Ca^{2+} ; (b) normalized spectra for the fluorescence of PCBMB and UV absorption of BAPTAVP; (c) UV-vis absorption spectra and (d) one-photon fluorescent spectra of BAPTAVP (B) when adding different volumes of PCBMB(P); inset in upper right corner of (d) is the fluorescent changing trend at 465 nm evolution with volumes of PCBMB.

The value is $0.982 \mu\text{mol/L}$, which is larger than those of some traditional Ca^{2+} probes, such as Fluo-3 ($K_d = 0.39 \mu\text{mol/L}$) [35]. This indicates that the BAPTAVP has a lower-affinity (higher K_d value) fluorescence probe for Ca^{2+} . Although the fluorescence indicators with high affinity (low K_d value) exhibit stronger fluorescence, the fluorescence change would be delayed because of the low dissociation. The fluorescence of the indicators easily reached saturation under the lower concentrations of Ca^{2+} , which would cause a larger deviation to analyze intracellular Ca^{2+} . As a result, the fluorescence probes

for intracellular Ca^{2+} with a lower affinity (higher K_d value) have been widely applied in fluorescence microscopy [33,36].

3.4. The Effects of Different Volumes of PCBMB on the Fluorescence of BAPTAVP

In Figure 2b, there are obvious overlaps between the fluorescence emission spectrum of PCBMB and UV absorption spectrum of BAPTAVP. According to the related literature [37,38], FRET may occur between the PCBMB (donor) and BAPTAVP (acceptor). To figure out the influence of adding PCBMB on the fluorescence of BAPTAVP, different volumes of PABMB were added to the solution of BAPTAVP in the tris-HCl buffer solution (10 mmol/L, KCl 100 mmol/L, pH 7.2) with a concentration of 1×10^{-5} mol/L, and the mole ratios of PCBMB to BAPTAVP (P:B) were 0, 0.2, 0.5, 1.0, 2.0, 3.0, 6.0, 10.0, 15.0, and 20.0. The UV-vis absorption spectra and OP fluorescence spectra are shown in Figure 2c,d, respectively. It can be seen from Figure 2c that the maximum absorption peak of BAPTAVP is at 420 nm, and that of PCBMB is at 325 nm. A new absorption peak at 340 nm appears when adding PCBMB into the solution of BAPTAVP. With the addition of PCBMB, the new absorption at 340 nm continuously increases, while the absorption of BAPTAVP at 420 nm gradually decreases and disappears. Similar phenomena are found in Figure 2d. A new fluorescence emission peak was obtained in comparison to those of BAPTAVP and PCBMB. The sharp bands at 528 nm are mainly the second harmonics of the beam source. Their amplitudes are enhanced with the increased concentrations of PCBMB, which have been reported in other studies [32,39]. Moreover, the fluorescent intensity increased dramatically with the addition of PCBMB before the ratio of polymer/probe = 1, and then levelled off. It was inferred that the self-assembly process between PCBMB with negative charges and BAPTAVP with positive charges was carried out by electrostatic interaction. Moreover, the charge transfer (CT) took place from electron donor (PCBMB) to electron acceptor (BAPTAVP), and the new blue-shift absorption peak and fluorescence emission peak appeared in comparison to those of BAPTAVP. A similar CT process was reported in the literature [40,41]. In addition, the distance between BAPTAVP and PCBMB will shorten after self-assembly, and extensive overlaps between the fluorescence emission spectrum of PCBMB and UV absorption spectrum of BAPTAVP in Figure 2b present an opportunity for FRET to greatly enhance the fluorescence of BAPTAVP. Furthermore, Figure 2d indicates that a steady complex of polymer-probe may form at the ratio of 1.0. This implies that the addition volume of PCBMB to achieve the ratio of BAPTAVP:PCBMB = 1:1 was optimal.

3.5. The Enhanced Fluorescence of Probe-Polymer System Detection of Ca^{2+}

OP fluorescent emission spectra of PCBMB, BAPTAVP, BAPTAVP- Ca^{2+} (1:1), PCBMB-BAPTAVP (1:1), and PCBMB-BAPTAVP- Ca^{2+} (1:1:1) are described in Figure 3a. The TP fluorescence of PCBMB was not found at 800 nm, which can be attributed to the poor absorbance at 400 nm (see Figure 2c). TP fluorescent spectra of the other four materials are shown in Figure 3b. Figure 3 shows that a new fluorescent emission band for PCBMB-BAPTAVP appeared in comparison to those of the original BAPTAVP and PCBMB, in both OP excitation and TP excitation. The experimental photophysical data are summarized in Table 1. The fluorescent quantum yields (Φ_s) and two-photon cross-sections ($\Phi\delta$) of the samples were measured by using coumarin307 in methanol ($\Phi = 0.56$, $\Phi\delta = 27.7$ GM at 800 nm) standard as the reference [42,43].

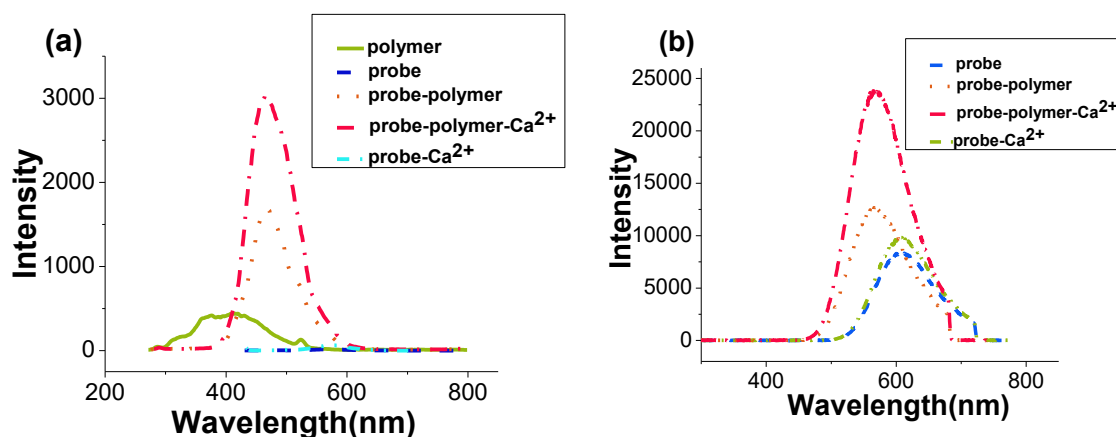


Figure 3. (a) One-photon (OP) and (b) TP fluorescent spectra of different systems. Polymer: PCBMB; probe: BAPTAVP.

Table 1. One- and two-photon relative photophysical data and zeta potentials of different systems ^[a].

Properties	Name				
	PCBMB	BAPTAVP	BAPTAVP-Ca ²⁺	PCBMB-BAPTAVP	PCBMB-BAPTAVP-Ca ²⁺
$\lambda_{\max}^{OP}/\lambda_{\max}^{TP}$ (nm)	416	573/606	574/606	467/569	468/569
Φ_s ^[c]	0.32	0.098	0.13	0.39	0.65
$\Phi\delta$ ^[d] (GM)	NF ^[e]	16.2	23.2	89	169
ZPs ^[f] (mV)	-52.1	10.5	27.5	46.4	-16.4

^[a] All data were measured with the concentrations of 10 $\mu\text{mol/L}$ for OP and 100 $\mu\text{mol/L}$ for TP tris-HCl buffer solution; ^[b] $\lambda_{\max}^{OP}/\lambda_{\max}^{TP}$ are emission wavelengths of OP and TP, respectively; ^[c] Φ_s is the fluorescence quantum yields; ^[d] $\Phi\delta$ is the TP active cross-section, $1\text{GM} = 10^{-50} \text{cm}^4\text{s photon}^{-1}$. The uncertainty is $\pm 10\%$; ^[e] Not found; ^[f] ZPs are zeta potentials of different systems; the concentrations of BAPTAVP, PCBMB, and Ca²⁺ are all 10 $\mu\text{mol/L}$.

The OP fluorescent peak of PCBMB-BAPTAVP was blue-shifted by 106 nm and red-shifted by 51 nm in comparison to those of original BAPTAVP and PCBMB, respectively, while its TP fluorescent peak was only blue-shifted by 37 nm in comparison to that of BAPTAVP. The reason may be attributed to the higher concentration ($1 \times 10^{-4} \text{mol/L}$) of the system solution to achieve reabsorption, and this influence was more remarkable for the system of PCBMB-BAPTAVP. The effect of concentration was investigated and is shown in Figure S1. The concentrations of the polymer-probe (PB:PCBMB:BAPTAVP = 1:1) were $5 \times 10^{-4} \text{mol/L}$ (PB-1), $1 \times 10^{-4} \text{mol/L}$ (PB-2), $5 \times 10^{-5} \text{mol/L}$ (PB-3), and $1 \times 10^{-5} \text{mol/L}$ (PB-4). The blue-shift degree of TP fluorescence peaks (PB-4, 475 nm; PB-3, 537 nm; PB-2, 569 nm; PB-1, 587 nm) will decline with increased concentrations of PCBMB-BAPTAVP versus the fluorescence emission peak of BAPTAVP. $\Phi\delta$ of BAPTAVP was slightly larger than that of coumarin 307 (15 GM) [43], and the fluorescent quantum yield was dramatically smaller than that of coumarin 307 (0.56), which indicates that the fluorescent properties of BAPTAVP were not very ideal. Considering CPs as TP fluorescent materials have a larger molar absorption coefficient, high fluorescence quantum yields, and outstanding TP cross-sections [44,45], we expected that the performance of BAPTAVP could be improved by doping a conjugate polymer with strong fluorescence. We can see that the fluorescence of BAPTAVP was greatly increased by combining PCBMB. In Table 1, the quantum yield and $\Phi\delta$ of PCBMB-BAPTAVP were increased by approximately 4 times (from 0.098 to 0.39) and 5.5 times (from 16.2 GM to 89 GM) in comparison to those of BAPTAVP, respectively. After adding Ca²⁺, the two values were 0.65 and 169, respectively, which indicates that the system of PCBMB-BAPTAVP was more sensitive to the detection of Ca²⁺.

3.6. Fluorescence Enhanced Mechanism

All those changes suggest that the fluorescence and sensitivity of the probe for Ca²⁺ can be effectively improved by combining PCBMB. The possible interaction mechanism was, furthermore, explored by TEM, DLS, and AFM, as shown in Figure 4 and Table 1. The average particle diameters

of PCBMB-BAPTAVP and PCBMB-BAPTAVP- Ca^{2+} were about 25 and 58 nm in Figure 4a,b, respectively, while that of pure BAPTAVP was not obtained, and the small molecule of BAPTAVP may be the source. In addition, TEM images in Figure 4e,f show that obvious sphere particles were found after adding the polymer of PCBMB. With the further addition of Ca^{2+} , the obvious aggregation of PCBMB-BAPTAVP particles will appear. This is coincident with the change in the particle diameters (from 25 nm of PCBMB-BAPTAVP to 58 nm of PCBMB-BAPTAVP- Ca^{2+}). The AFM images present clearer evidence in Figure 4g–l. The nanoparticle sizes of PCBMB-BAPTAVP are more uniform. The obvious aggregation was found after the addition of Ca^{2+} . Furthermore, the ZPs of different systems including PCBMB, BAPTAVP, BAPTAVP- Ca^{2+} , PCBMB-BAPTAVP, and PCBMB-BAPTAVP- Ca^{2+} were measured in Table 1. The concentrations of PCBMB, BAPTAVP, and Ca^{2+} are the same as 10 $\mu\text{mol/L}$. In Table 1, the ZP of PCBMB-BAPTAVP (-46.4 mV) is a median between that of PCBMB (-52.1 mV) and BAPTAVP (10.5 mV), which shows that self-assembly may take place between positive charges of BAPTAVP and negative charges of PCBMB. TEM and AFM results further indicate that the self-assembly sphere particles were formed by the coiling from the long polymer chain. Meanwhile, FRET between BAPTAVP and PCBMB greatly increased the fluorescence of BAPTAVP. Adding Ca^{2+} , the ZPs of BAPTAVP and PCBMB-BAPTAVP are both enhanced from 10.5 to 27.5 mV for BAPTAVP and from -46.4 to 16.4 mV for PCBMB-BAPTAVP, which shows that BAPTAVP captured Ca^{2+} to effectively increase the fluorescence (23.2 GM for the $\Phi\delta$ of BAPTAVP- Ca^{2+} , 169 GM for the $\Phi\delta$ of PCBMB-BAPTAVP- Ca^{2+}). In addition, the ^1H NMR spectra of BAPTAVP, BAPTAVP-added acetylcholine esterase, BAPTAVP-added acetylcholine esterase, and Ca^{2+} were measured and are shown in Figure S2. We can see that the carboxyl groups appear in the presence of acetylcholine esterase because of hydrolysis of ester bonds in BAPTAVP (Figure S2B). Furthermore, the carboxyl groups will disappear after the addition of Ca^{2+} because of coordination with BAPTAVP, which enhances the fluorescence of BAPTAVP by attenuating the intramolecular charge transfer process [32]. Based on the above results, the possible interaction mechanism is described in Scheme 1.

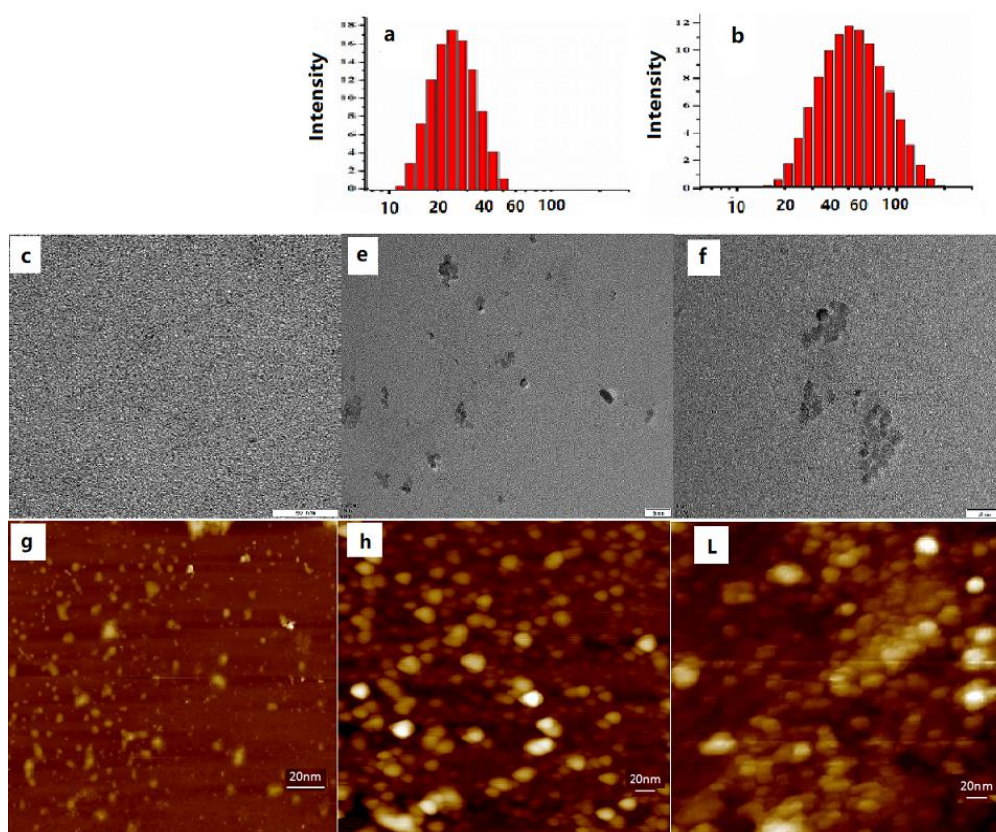


Figure 4. Particle size distribution of (a) PCBMB-BAPTAVP (1:1) and (b) PCBMB-BAPTAVP- Ca^{2+}

(1:1:1); TEM and atomic force microscopy (AFM) images of (c,g) BAPTAVP, (e,h) PCBMB-BAPTAVP (1:1), and (f,i) PCBMB-BAPTAVP-Ca²⁺ (1:1:1), respectively. The concentrations of PCBMB, BAPTAVP, and Ca²⁺ are all 10 μ M.

3.7. Fluorescence Microscopy Imaging

The potential application of the PCBMB-BAPTAVP system for the detection of Ca²⁺ in living cells by TPM was investigated (shown in Figure 5). SiHa cells were incubated with 5 μ mol/L of BAPTAVP or PCBMB-BAPTAVP for 1 h at room temperature and then washed with PBS three times. The fluorescence of BAPTAVP was collected in the range of 520–620 nm (λ_{ex} = 800 nm) with a power of 6%, whereas the fluorescence of PCBMB-BAPTAVP was collected in the range of 450–520 nm at 800 nm with a power of 2.5%, which can avoid the disturbance from the fluorescence of BAPTAVP. Obvious fluorescence from the intracellular area was found when the cells were incubated with the PCBMB-BAPTAVP system at a lower power (shown in Figure 5c), which is different from the poor fluorescence of BAPTAVP (shown in Figure 5a). Furthermore, after the cells were supplemented with 5 μ mol/L of Ca²⁺ under the same condition, obvious fluorescence of both BAPTAVP and PCBMB-BAPTAVP was found (shown in Figure 5b,d). However, a significantly enhanced fluorescence of the PCBMB-BAPTAVP system from the intracellular area was observed (shown in Figure 5d). The above results indicate that the PCBMB-BAPTAVP system could detect endogenous Ca²⁺ in living cells and was more sensitive.

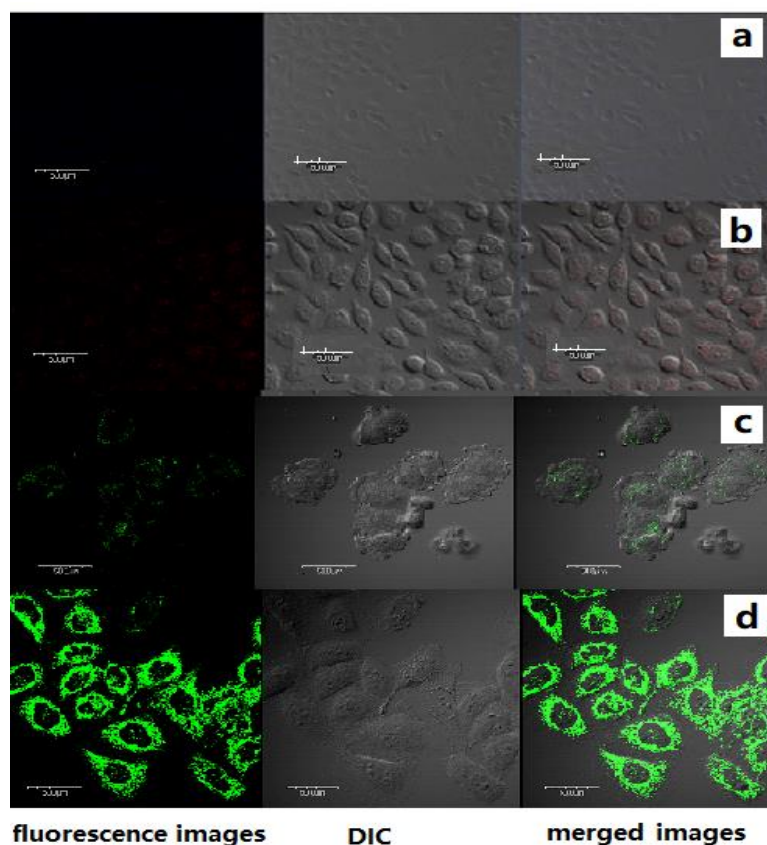


Figure 5. TP fluorescence (left), DIC (Differential interference contrast, middle), and merged (right) images of SiHa cells were incubated for 1 h at 37 °C with different systems including (a) BAPTAVP (5 μ mol/L); (b) BAPTAVP (5 μ mol/L)-Ca²⁺ (5 μ mol/L); (c) PCBMB (5 μ mol/L)-BAPTAVP (5 μ mol/L); and (d) PCBMB (5 μ mol/L)-BAPTAVP (5 μ mol/L)-Ca²⁺ (5 μ mol/L). The excited wavelength was 800 nm. The scale bar in a-d is all of 500 μ m.

4. Conclusions

In conclusion, a novel probe with BAPTA as the chelating group and a CP of carbazole derivative were synthesized and characterized. The data including TEM, AFM, DLS, ZPs, $^1\text{H NMR}$, and fluorescence spectra showed that the nanoparticles were formed by the self-assembly between positive charges of BAPTAVP and negative charges of PCBMB, which effectively increased the fluorescent properties of BAPTAVP (from 0.098 to 0.39 for Φ ; from 16.2 to 89 GM for $\Phi\delta$) by fluorescence resonance energy transfer (FRET) with PCBMB and attenuating the intramolecular charge transfer (ICT) after the addition of Ca^{2+} . The $\Phi\delta$ of PCBMB-BAPTAVP- Ca^{2+} was up to 169 GM. Furthermore, the excellent fluorescence properties of PCBMB-BAPTAVP to detect intracellular Ca^{2+} were demonstrated by TPM. This method may provide a new way to design the system of metal ion detection with better fluorescence.

Supplementary Materials: The following are available online at <http://www.mdpi.com/2073-4360/11/10/1643/s1>.

Author Contributions: Y.-I.Z. and Q.-b.W. conceived and planned the experiments. Y.-I.Z., Q.-b.W. and H.Y. carried out the experiments and contributed to sample preparation. X.Z. contributed to the interpretation of the results. Q.-b.W. and X.-y.J. took the lead in writing the Original Draft Preparation. All authors provided critical feedback and helped shape the research, analysis, and manuscript. X.Z. is the project administration and funding acquisition.

Funding: This project was supported by the National Natural Science Foundation of China (NSFC 51403111, 11774188) and Sichuan Provincial Science and Technology Innovation Talents (2018RZ0113).

Acknowledgments: We are particularly grateful to the funding supporting from Qilu University of Technology for talents.

Conflicts of Interest: There is no conflict of interest regarding the publication of this manuscript.

References

1. Mohan, P.S.; Lim, C.S.; Tian, Y.S.; Roh, W.Y.; Lee, J.H.; Cho, B.R. A two-photon fluorescent probe for near-membrane calcium ions in live cells and tissues. *Chem. Commun.* **2009**, *36*, 5365–5367. [[CrossRef](#)] [[PubMed](#)]
2. Wu, Y.X.; Li, J.B.; Liang, L.H.; Lu, D.Q.; Zhang, J.; Mao, G.J.; Zhou, L.Y.; Zhang, X.B.; Tan, W.; Shen, G.L.; et al. A rhodamine-appended water-soluble conjugated polymer: An efficient ratiometric fluorescence sensing platform for intracellular metal-ion probing. *Chem. Commun.* **2014**, *50*, 2040–2042. [[CrossRef](#)] [[PubMed](#)]
3. Liu, Z.C.; Jing, X.; Zhang, S.J.; Tian, Y. A copper nanocluster-based fluorescent probe for real-time imaging and ratiometric biosensing of calcium ions in neurons. *Anal. Chem.* **2019**, *91*, 2488–2497. [[CrossRef](#)] [[PubMed](#)]
4. Berridge, M.J.; Lipp, P.; Bootman, M.D. The versatility and universality of calcium signaling. *Nat. Rev. Mol. Cell. Biol.* **2000**, *1*, 11–21. [[CrossRef](#)] [[PubMed](#)]
5. Carafoli, E.; Santella, L.; Branca, D.; Brini, M. Generation, control, and processing of cellular calcium signals. *Crit. Rev. Biochem. Mol.* **2001**, *36*, 107–260. [[CrossRef](#)] [[PubMed](#)]
6. Bootman, M.D.; Berridge, M.J. The elemental principles of calcium signaling. *Cell* **2009**, *83*, 675–678. [[CrossRef](#)]
7. Berridge, M.J.; Bootman, M.D.; Roderick, H.L. Calcium signalling: Dynamics, homeostasis and remodeling. *Nat. Rev. Mol. Cell. Biol.* **2003**, *4*, 517–529. [[CrossRef](#)] [[PubMed](#)]
8. Shin, Y.N.; Lim, C.S.; Tian, Y.S.; Rho, W.Y.; Cho, B.R. Detection of near-membrane calcium ions in live tissues with a two-photon fluorescent probe. *Bull. Korean Chem. Soc.* **2010**, *31*, 599–605. [[CrossRef](#)]
9. Eggeling, C.; Volkmer, A.; Seidel, C.A.M. Molecular photobleaching kinetics of rhodamine 6G by one- and two-photon induced confocal fluorescence microscopy. *ChemPhysChem* **2005**, *6*, 791–804. [[CrossRef](#)] [[PubMed](#)]
10. Kim, D.; Moon, H.; Baik, S.H.; Singha, S. Two-photon absorbing dyes with minimal autofluorescence in tissue imaging: Application to in vivo imaging of amyloid- β plaques with a negligible background signal. *J. Am. Chem. Soc.* **2015**, *137*, 6781–6789. [[CrossRef](#)] [[PubMed](#)]
11. Lim, C.S.; Kang, M.Y.; Han, J.H.; Danish, I.A.; Cho, B.R. In vivo imaging of near-membrane calcium ions with two-photon probes. *Chem. Asian. J.* **2011**, *6*, 2028–2033. [[CrossRef](#)] [[PubMed](#)]
12. Tojyo, Y.; Tanimura, A.; Matsumoto, Y. Monitoring of Ca^{2+} release from intracellular stores in permeabilized rat parotid acinar cells using the fluorescent indicators mag-fura-2 and calcium green C18. *Biochem. Biophys. Res. Commun.* **1997**, *240*, 189–195. [[CrossRef](#)]

13. Park, H.; Hoang, D.T.; Paeng, K.; Kaufman, L.J. Localizing exciton recombination sites in conformationally distinct single conjugated polymers by super-resolution fluorescence imaging. *ACS Nano*. **2015**, *9*, 3151–3158. [[CrossRef](#)] [[PubMed](#)]
14. Ruan, Z.; Yuan, P.; Li, T.; Tian, Y.; Cheng, Q.; Yan, L. Glutathione triggered near infrared fluorescence imaging-guided chemotherapy by cyanine conjugated polypeptide. *ACS Biomater. Sci. Eng.* **2018**, *4*, 4208–4218. [[CrossRef](#)]
15. Wu, C.; Szymanski, C.; Cain, Z.; McNeill, J. Conjugated polymer dots for multiphoton fluorescence imaging. *J. Am. Chem. Soc.* **2007**, *129*, 12904–12905. [[CrossRef](#)]
16. Li, S.; Jiang, X.F.; Xu, Q.H. Conjugated polymers for two-photon live cell imaging. In *Conjugated Polymers for Biological and Biomedical Applications*; Liu, B.L., Ed.; Willey: Hoboken, NJ, USA, 2018; pp. 135–170.
17. Wei, L.; Zhang, D.; Zheng, X.; Zeng, X.; Zeng, Y.; Shi, X.; Shu, X.; Xiao, L. Fabrication of positively charged fluorescent polymer nanoparticles for cell imaging and gene delivery. *Nanotheranostics* **2018**, *2*, 157–167. [[CrossRef](#)] [[PubMed](#)]
18. Meng, X.L.; Zhang, X.; Yao, J.S.; Zhang, J.J.; Ding, B.Y. Fluorescence and fluorescence imaging of two Schiff derivatives sensitive to Fe³⁺ induced by single- and two-photon excitation. *Sens. Actuators B Chem.* **2013**, *176*, 488–496. [[CrossRef](#)]
19. Gao, Z.Y.; Zhang, C.J.; Zhang, X.; Xing, S.; Yao, J.S.; Qiao, C.D.; Liu, W.L. A new “turn-on” fluorescence probe for Al³⁺ detection and application exploring in living cell and real samples. *Appl. Sci.* **2019**, *9*, 577. [[CrossRef](#)]
20. Kim, H.J.; Lim, C.S.; Lee, H.W.; Lee, H.S.; Um, Y.J.; Han, I.; Kim, M.K. A ratiometric two-photon probe for Ca²⁺, in live tissues and its application to spinal cord injury model. *Biomaterials* **2017**, *141*, 251–259. [[CrossRef](#)]
21. Zhao, X.J.; Wang, C.; Yuan, G.Q.; Ding, H.Y.; Zhou, L.Y.; Liu, X.Q. A dual-site modulated FRET-based two-photon ratiometric fluorescent probe for tracking lysosomal pH changes in living cells, tissues and zebrafish. *Sens. Actuators B Chem.* **2019**, *290*, 79–86. [[CrossRef](#)]
22. Zhang, C.J.; Gao, Z.Y.; Wang, Q.B.; Zhang, X. Highly sensitive detection of melamine based on the fluorescence resonance energy transfer between conjugated polymer nanoparticles and gold nanoparticles. *Polymers* **2018**, *10*, 873. [[CrossRef](#)] [[PubMed](#)]
23. Sha, J.; Song, Y.; Liu, B.X.; Lü, C.L. Host–guest-recognition-based polymer brush-functionalized mesoporous silica nanoparticles loaded with conjugated polymers: A facile FRET-based ratiometric probe for Hg²⁺. *Micropor. Mesopor. Mater.* **2015**, *218*, 137–143. [[CrossRef](#)]
24. Gryniewicz, G.; Poenie, M.; Tsien, Y. A new generation of Ca²⁺ indicators with greatly improved fluorescence properties. *J. Biol. Chem.* **1985**, *260*, 3440–3450. [[PubMed](#)]
25. Zhao, C.F.; He, G.S.; Bhawalkar, J.D.; Park, C.K.; Prasad, P.N. Newly synthesized dyes and their polymer/glass composites for one- and two-photon pumped solid-state cavity lasing. *Chem. Mater.* **1995**, *7*, 1979–1983. [[CrossRef](#)]
26. Zhang, X.; Sun, Y.; Yu, X.Q.; Zhang, B.Q.; Huang, B.B.; Jiang, M.H. Synthesis and nonlinear optical properties of several new two-photon photopolymerization initiators about dibenzothiophene derivatives. *Syn. Met.* **2009**, *159*, 2491–2496. [[CrossRef](#)]
27. Wu, Q.Q.; Song, Q.H. Photosensitized splitting of thymine dimer or oxetane unit by a covalently N-linked carbazole via electron transfer in different Marcus regions. *J. Phys. Chem. B* **2010**, *114*, 9827–9832. [[CrossRef](#)] [[PubMed](#)]
28. Danish, I.A.; Lim, C.S.; Tian, Y.S.; Han, J.H.; Kang, M.Y.; Cho, B.R. Two-photon probes for Zn²⁺ ions with various dissociation constants. Detection of Zn²⁺ ions in live cells and tissues by two-photon microscopy. *Chem. Asian J.* **2011**, *6*, 1234–1240. [[CrossRef](#)] [[PubMed](#)]
29. Thomas, S.W.; Joly, G.D.; Swager, T.M. Chemical sensors based on amplifying fluorescent conjugated polymers. *Chem. Rev.* **2007**, *107*, 1339–1386. [[CrossRef](#)]
30. Wang, H.; Li, Z.; Shao, P.; Qin, J.; Huang, Z.L. Two-photon absorption property of a conjugated polymer: Influence of solvent and concentration on its property. *J. Phys. Chem. B* **2009**, *114*, 22–27. [[CrossRef](#)]
31. Liu, Y.; Qiao, Q.; Zhao, M.; Yin, W.; Miao, L.; Wang, L.; Xu, Z. Cd²⁺-triggered amide-tautomerization produces a highly Cd²⁺-selective fluorescent sensor across a wide pH range. *Dyes Pigment.* **2016**, *133*, 339–344. [[CrossRef](#)]

32. Gao, Z.Y.; Zhang, X.; Xing, S.; Lu, Q.; Yao, J.S.; Liu, Q.Z.; Qiao, C.D.; Xie, R.X.; Ding, B.Y. Conjugated polymer nanoparticles based on carbazole for detecting ferric ion (III) with a large Stokes shift and high sensitivity and the application in cell imaging. *Dyes Pigment.* **2019**, *168*, 68–76. [[CrossRef](#)]
33. Sui, B.L.; Liu, X.L.; Wang, M.Y.; Belfield, K.D. A highly selective fluorescence turn-on sensor for extracellular calcium ion detection. *Chem. Eur. J.* **2016**, *22*, 10351–10354. [[CrossRef](#)]
34. Zhang, X.; Li, L.L.; Liu, Y.K. Fluorescent detection and imaging of Hg²⁺ using a novel phenanthroline derivative based single- and two-photon excitation. *Mater. Sci. Eng. C* **2016**, *59*, 916–923. [[CrossRef](#)] [[PubMed](#)]
35. Rockwell, P.L.; Storey, B.T. Determination of the intracellular dissociation constant, K(D), of the fluo-3. Ca (2+) complex in mouse sperm for use in estimating intracellular Ca(2+) concentrations. *Mol. Reprod. Dev.* **1999**, *54*, 418–428. [[CrossRef](#)]
36. Zhao, M.; Hollingworth, S.; Baylor, S.M. Properties of tri- and tetracarboxylate Ca²⁺ indicators in frog skeletal muscle fibers. *Biophys. J.* **1996**, *70*, 896–916. [[CrossRef](#)]
37. Li, S.; Shen, X.; Li, L.; Yuan, P.; Guan, Z.; Yao, S.Q.; Xu, Q.H. Conjugated-polymer-based red-emitting nanoparticles for two-photon excitation cell imaging with high contrast. *Langmuir* **2014**, *30*, 7623–7627. [[CrossRef](#)]
38. Ding, D.S.; Lu, Z.H. The second harmonic component in the Bessel beam. *Appl. Phys. Lett.* **1996**, *68*, 608–610. [[CrossRef](#)]
39. Matsui, P.; Sadhu, K.K.; Mizukami, S.; Kikuchi, K. Highly selective tridentate fluorescent probes for visualizing intracellular Mg²⁺ dynamics without interference from Ca²⁺ fluctuation. *Chem. Commun.* **2017**, *53*, 10644–10647. [[CrossRef](#)]
40. Xu, Z.; Xiao, Y.; Qian, X.; Cui, J.; Cui, D. Ratiometric and selective fluorescent sensor for Cu (II) based on internal charge transfer (ICT). *Org. Lett.* **2005**, *7*, 889–892. [[CrossRef](#)]
41. Wang, J.B.; Qian, X.F.; Cui, J.N. Detecting Hg²⁺ ions with an ICT fluorescent sensor molecule: Remarkable emission spectra shift and unique selectivity. *J. Org. Chem.* **2006**, *71*, 4308–4311. [[CrossRef](#)]
42. Li, L.L.; Zhang, X.; Zhang, W.J.; Li, W.; Sun, W.H.; Redshaw, C. Zinc 2-((2-(benzoimidazol-2-yl)quinolin-8-ylimino) methyl) phenolates: Synthesis, characterization and photoluminescence behavior. *Spectrochim. Acta A Mol. Biomol. Spectrosc.* **2014**, *118*, 1047–1055. [[CrossRef](#)]
43. Chris, X.; Webb, W.W. Measurement of two-photon excitation cross sections of molecular fluorophores with data from 690 nm to 1050 nm. *Opt. Soc. Am.* **1996**, *13*, 481–491.
44. Huang, F.; Tian, Y.; Chen, C.Y.; Cheng, Y.J.; Young, C.A.; Jen, A.K.Y. Cross-conjugated polymers with large two-photon absorption cross-sections for metal ion sensing. *J. Phys. Chem. C* **2007**, *111*, 10673–10681. [[CrossRef](#)]
45. Hu, L.W.; Liang, L.; Yong, Y. Green-emitting polyfluorenes containing hexylthiophen-dibenzothiophene-S, S-dioxide unit with large two-photon absorption cross section. *Chin. J. Polym. Sci.* **2018**, *36*, 546–554. [[CrossRef](#)]

